

Contents lists available at [Egyptian Knowledge Bank](https://www.egyptianknowledgebank.com/)

Labyrinth: Fayoum Journal of Science and Interdisciplinary Studies

Journal homepage: <https://ifsis.journals.ekb.eg/>

Characterization of Different Metal Oxides Thin Films Deposited by Spin Coating Technique

Adel M. El Sayed^{a,*}, Mohamed Shaban^{b,c}, G. Said^a^aPhysics Department, Faculty of Science, Fayoum University, El-Fayoum 63514, Egypt^bDepartment of Physics, Faculty of Science, Islamic University of Madinah, Madinah 42351, Saudi Arabia^cNanophotonics and Applications (NPA) Lab, Department of Physics, Faculty of Science, Beni-Suef University, Beni-Suef 62514, Egypt

ARTICLE INFO

Keywords:

Metal Oxide Semiconductors Transparent
Conducting Oxides Spin-coating
Bandgap
Refractive Index
Spinel Structure.

ABSTRACT

Designing and building up nanostructures that exhibit outstanding optical, electrical, mechanical, and magnetic properties, compared to bulk materials is attracting increasing attention worldwide. This work is an attempt to fabricate and characterize different metal oxides (MO) in the form of thin films that are applicable in diverse fields of industry and technology. Cobalt oxide (Co₃O₄), copper oxide (CuO), iridium oxide (IrO₂), zinc oxide (ZnO), and cadmium oxide (CdO) thin films were prepared by the sol-gel method utilizing the spin-coating technique. The crystal structure of the films was analyzed by XRD. The films' morphology was investigated by AFM/FE-SEM. The optical properties of the films were studied in detail. XRD results indicated the high purity and good crystallinity of the prepared films. XRD and FE-SEM/AFM revealed the nanoscale and grain size of the films as well as their surface morphology and roughness. UV-vis-NIR spectroscopy was utilized to evaluate the optical properties and band structure of all films. ZnO and CdO films showed higher transmittance (79–89%) compared to about 62% for the other films. The optical band gap of the films was found to be in the range of 1.7–3.2 eV. The refractive index of the films was evaluated. The sol-gel spin-coated films are the best candidates for modern applications, including hydrogen production by water splitting, gas sensing, and optoelectronic applications.

1. Introduction

MO are considered promising materials for various technological applications. The low cost, abundance, stability, resistance to photo-corrosion, electronic structure, light absorption properties, and charge transport features are general advantages for these oxides [1,2]. This is besides their different kinds, simple preparation routes, and environmental friendliness [3]. At the nanoscale, the increased specific surface area, high surface energy, reduced imperfections, and the effects of confinement arising from the nano-structuration modify these advantages and improve the physicochemical properties of MO, widening their multi-functionality [4–8].

Among the MO, cobalt oxide (Co₃O₄) exhibits unique physical (optical, magnetic, and electrical) properties owing to the metal cation's multivalence, high electrochromism, *i.e.*, improved cathodic bleaching and anodic coloration efficiency. Moreover, Co₃O₄ has a small bandgap of about 2.1 eV which make it suitable for the photonic devices. Co₃O₄ can be used as an effective hole transport, where it is a p-type semiconductor that adsorbs the O₂ from the air at the ambient conditions and forms surface states [9, 10]. These properties encouraged the use of Co₃O₄ for energy devices (batteries), solar selective absorbers, high-contrast displays, smart windows, water-splitting, and gas sensing [4, 10–12]. Additionally, CuO is abundant, exhibits interesting electrical, and optical properties, has chemical stability, and is environmentally safe. It is monoclinic, has a narrow E_g^{op} (1.10–1.71 eV) and could achieve solar conversion efficiency of up to 33% for a single-junction PV cell [13,14]. In addition, CuO is used in various fields of science and technology, including magnetic storage media, Na-ion batteries, gas sensing, photocatalysis, and photoelectrochemical cells [15]. Moreover, CuO has been used in antimicrobial applications and nanofluid preparation [16].

Another MO is iridium oxide (IrO₂), which displays exceptional thermal stability and chemical resistivity towards aggressive basic or acidic media. Moreover, its interesting electrochemical and optoelectronic properties make it the best choice for electrochromic displays, optical switching, automobile rear-view mirrors, pH monitoring, as an electrocatalyst for the oxygen evolution reaction and anodic reaction in water electrolysis, and has been used in the chloralkali industry [17–20].

* Corresponding author.

E-mail address: ash02@fayoum.edu.eg (A. Hassen); Tel.: +201001104150DOI: [10.21608/ifsis.2023.301867](https://doi.org/10.21608/ifsis.2023.301867)

Received 10 March 2023; Received in revised form 8 April 2023; Accepted 8 April 2023

Available online 26 April 2023

All rights reserved

A special class of MO that combines good electrical conductivity with high optical transparency is named transparent conducting oxides (TCO), such as ZnO, and CdO. Film deposition and technology based on TCO attract increasing attention due to their application in various industrial fields and engineering. Zinc oxide (ZnO) is also TCO, which is the second most widely studied semiconductor material after Si [21]. Its direct wide E_g^{op} of 3.25 eV and large exciton binding energy (60 meV) allowed us to consider ZnO as a next-generation light-emitting diode (LED) [22]. The hexagonal structure of ZnO displays a strong spontaneous piezoelectric polarization [21]. ZnO can block UV light and exhibits a relatively high electrical conductivity and high transmittance in the visible region, which makes this material suitable for paints, cosmetics [23], as a front contact for dye-sensitized solar cells [24], and for photocatalytic dye degradation in both basic and acidic media [25]. CdO is another interesting II–VI TCO, with high electrical conductivity of $\sim 10^3 \Omega^{-1} \text{ cm}^{-1}$, high mobility of $\sim 146 \text{ cm}^2 \text{ V}^{-1} \text{ s}^{-1}$, and carrier concentration of $\sim 1.5 \times 10^{20} \text{ cm}^{-3}$, high transmittance in the visible region, and high reflectance in the infrared region. Its E_g^{op} is between 2.2 and 2.6 eV, depending on Cd interstitial $\text{Cd}_{(1+x)}\text{O}$ or O vacancies $\text{CdO}_{(1-x)}$ [26,27]. These properties encouraged the use of CdO in heat mirrors/antireflection coatings, pigments, phototransistors, CdO/Cu₂O solar cells, photoelectrochemical (PEC) devices, IR detectors, and gas sensors [28, 29].

Various chemical and physical routes have been used for preparation of MO thin films. Balakarthikeyan et al. [30] developed Co₃O₄ for photo-detector application by tuning the coating temperature through the spray pyrolysis method. Tso et al. [31] fabricated Na-doped IrO₂ thin film, by a sequential oxidative–reductive technique, with an improved bio-sensing and bio-stimulating performance. C.-Guzmán et al. [32] utilized a photo-deposition technique to prepare CuO-loaded ZnO. At 1.0 % CuO loading, the ZnO film showed enhanced photocatalytic degradation of rhodamines. Therefore, this construction is suitable for waste water treatment. Abd El-Moula et al.[33] developed CdO/Cu/CdO thin film multilayers, applying the DC pulsed plasma sputtering technique, for some optoelectronics self-cleaning applications. Among the used techniques for the thin film fabrication, the sol-gel spin-coating technique has some unique advantages, including the simplicity, low cost, easy adjusting composition, simple deposition equipment, fabricating large-area films, the easy preparation of a homogeneous mixture of two cations in the liquid state, and the non-use of any volatile compounds. Thus, it is an ideal technique from an economic point of view and for safe handling reasons [34].

Owing to the technological importance and applications of Co₃O₄, CuO, IrO₂, ZnO, and CdO, the work represents an attempt to prepare pure films of nano-sized structures, utilizing one method, *i.e.*, the sol-gel spin coating technique, and different precursor materials. XRD, AFM and FE-SEM were used to investigate the structure and surface morphology of the films and UV-vis spectroscopy was used to study the optical properties and band structure of the films. Different applications were proposed for the prepared materials and more attempts will be carried out to develop the films properties to improve their performance and broaden their industrial applications.

2. Experimental part

2.1. Materials and preparation

The preparation process is described in the flowchart of Fig.1. The 0.25 M solutions were prepared by dissolving the required amount from the acetate salts; cobalt acetate tetrahydrate $[(\text{CO}_2\text{CH}_3)_2\text{Co}\cdot 4\text{H}_2\text{O}]$, 249.1 g/mol, Merck], Cu (II) acetate monohydrate $[\text{Cu}(\text{CO}_2\text{CH}_3)_2\cdot \text{H}_2\text{O}]$, ~ 200 g/mol, PRS Panreac, Spain], $[\text{Zn}(\text{CO}_2\text{CH}_3)_2\cdot 2\text{H}_2\text{O}]$, 219.5 g/mol, Panreac], or cadmium acetate dihydrate $[\text{CdCO}_2(\text{CH}_3)_2\cdot 2\text{H}_2\text{O}]$, $M_w=266.52$ g/mole, Merck]. 10 ml of 2-methoxyethanol ($\text{C}_3\text{H}_8\text{O}_2$) as a solvent and monoethanol amine ($\text{C}_2\text{H}_7\text{NO}$, MEA) as a stabilizer was added to each salt. In the case of IrO₂ film, 0.1 M solution was prepared by dissolving $\text{IrCl}_3\cdot x\text{H}_2\text{O}$ [298.58 g/mol, Spira Chemical] in 10 ml ethanol without using the stabilizing agent. The glass substrate was cleaned using detergents, acetone, and clean water in an ultrasonic bath, in separate steps for 10 min for each, and finally dried using hot air.

2.2. Measurements

The structure and crystal phase identification of the films studied by X-ray diffraction (XRD) technique and the device supplied by Philips X'Pert Pro MRD that apply Cu K_α radiation of wavelength $\lambda \sim 1.542 \text{ \AA}$. The surface morphology of the films was investigated using the atomic force microscope (AFM) supplied by PARK, XE-100E, and field emission-scanning electron microscope (ZEISS SUPRA 55 VP, ZEISS LEO, Gemini Column). The UV-vis absorbance/transmittance spectra of the films were recorded in the wavelength range of 200–1500 nm using SHIMADZU UV-3600 UV–Vis–NIR spectrophotometer at RT.

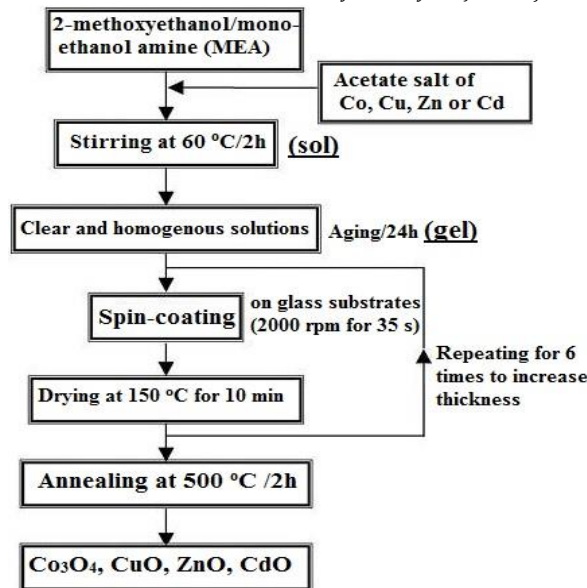


Fig.1: Flowchart of the sol-gel spin coating preparation procedures [6,7].

3. Results and discussion

3.1. XRD analysis

The X-ray diffraction patterns of the sol-gel spin-coated films after annealing at 500 °C for 2h are shown in Fig. 2. The appearance of several diffraction peaks means that the films are polycrystalline and the grains were grown in random orientations during the progression of the films [35]. Fig. 2(a) shows some crystalline peaks at $2\theta = 31.56^\circ, 36.55^\circ, 45.38^\circ, 56.1^\circ,$ and 65.42° , which are correspond to (2 2 0), (3 1 1), (4 0 0), (4 2 2), and (4 4 0) planes of Co_3O_4 with a spinel face-centered cubic (fcc) structure and belong to the space group (SG) $\text{Fd}\bar{3}m$. This result is consistent with the reference JCPDS code: 01-80-1542. No peaks related to other cobalt oxides like CoO and Co_2O_3 are found in this pattern. This indicates that annealing at 500 °C was enough to get the stable phase (Co_3O_4). Fig. 2 (b) is the XRD spectra of CuO thin film, where all the diffraction peaks are indexed to a $\text{C}2/c$ SG of CuO with a monoclinic system and according to JCPDS No. 45-0937. The peak at $2\theta = 35.49^\circ$ and that at 38.67° are owing to the reflecting (0 0 2) and (2 0 0) planes of CuO of a monoclinic structure, respectively. The preferred growth in these two directions, indicated by the high intensity of these two peaks, illustrates that the deposited CuO film is thermodynamically stable [36, 37]. The crystallite size (C_s) of the deposited films was calculated based on the values of full-width at half maximum (FWHM) of the most intense reflections and by using Debye-Scherrer's equation; $C_s = 0.9\lambda/\text{FWHM} \cos\theta$, where FWHM is in radians, θ is the Bragg's angle. The average C_s values of all films are listed in Table 1.

The average C_s of Co_3O_4 and CuO are 17.25 and 22.5 nm. Moreover, for the cubic Co_3O_4 , the lattice parameter (a) is determined from the relation $a = d_{(hkl)}\sqrt{h^2 + k^2 + l^2}$, whereas, for the monoclinic system, the equation is more complicated and given by [38]: $\frac{1}{d^2} = \frac{1}{\sin^2\beta} \left(\frac{h^2}{a^2} + \frac{k^2}{b^2} \sin^2\beta + \frac{l^2}{c^2} - \frac{2hl \cos\beta}{ac} \right)$, where ($h k l$) are the Miller indices written above the diffraction peaks as indicated in Fig.1. The value of a of Co_3O_4 is 8.121 Å, and the lattice parameters (a , b and c) of CuO are found to be 4.720 Å, 3.431 Å, and 5.128 Å, respectively. Fig. 2 (c) shows the XRD pattern of IrO_2 film, where small crystalline peaks at $2\theta \approx 27.78^\circ, 35^\circ, 41^\circ$ and 54° correspond to (1 1 0), (1 0 1), (2 0 0) and (2 1 1) planes, according to JCPDS card no. 01-086-0330. The observed peaks and their positions indicate the formation of iridium (IV) oxide, or tetragonal IrO_2 . Similar results were reported by Uzgören et al. [39] for electrolysis-deposited films. Fig. 2(d) shows that the ZnO film of polycrystalline Wurtzite (hexagonal) structure, SG $\text{C}_{6v}=\text{P}6_3\text{mc}$, is consistent with JCPDS-89-0510 [40, 41].

The C_s of ZnO were determined considering the three most intense peaks (1 0 0), (0 0 2), and (1 0 1) and found to be 34.21 nm. In addition, the lattice constants (a and c) of the hexagonal ZnO can be calculated by using the equation [42]: $d_{(hkl)} = 1/\left[\frac{1}{3}\left(\frac{h^2+k^2+hk}{a^2}\right) + \frac{l^2}{c^2}\right]^{0.5}$, which can be rewritten for (1 0 1) and (0 0 2) as $d_{(101)} = \left[\frac{1}{3}\left(\frac{1}{a^2}\right) + \frac{1}{c^2}\right]^{-0.5}$ and $d_{(002)} = \frac{c}{2}$. The a and c values were found to be 3.254 Å and 5.21 Å, respectively. The diffraction peaks of Fig. 2 (e) belong to the cubic phase of CdO with a lattice parameter $a = 4.695$ Å and SG $\text{Fm}\bar{3}m$. The ($h k l$) peaks at $2\theta = 33.1^\circ, 38.4^\circ,$ and 55.4° are matching the (1 1 1), (2 0 0), and (2 2 0) plans, respectively, according to JCPDS file No. 75-0592. This indicates the formation of well-crystallized CdO of high purity [43], where the precursor has completely transformed into the CdO phase. The C_s average value obtained is 59.8 nm.

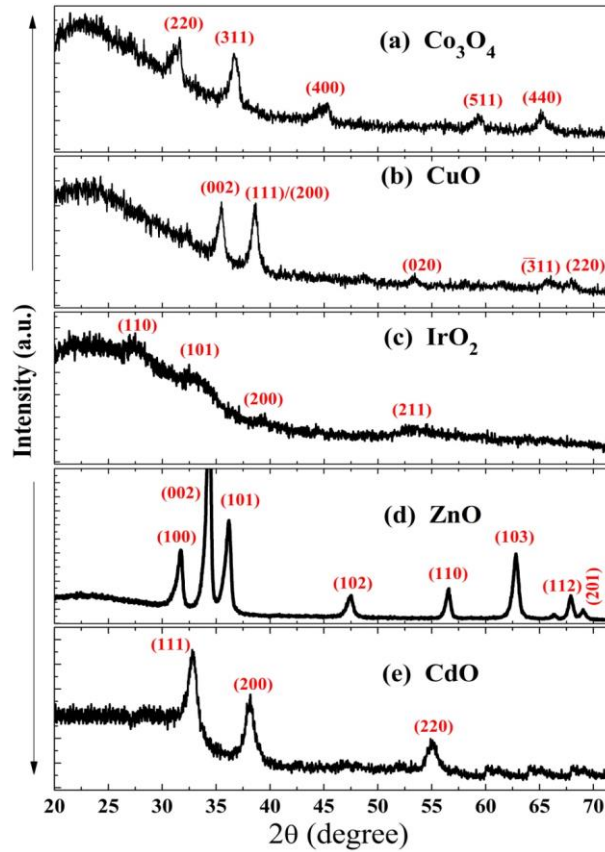


Fig.2: (a-e) XRD diffraction patterns of the sol-gel spin coating Co_3O_4 , CuO , IrO_2 , ZnO , and CdO films.

Table 1: The crystallite size (C_s), lattice parameters (a, b, c), particle size (D), transmittance ($T\%$) and reflectance ($R\%$) at 700 nm, band gap (E_g^{op}) and the refractive index (n) of the films:

Film	C_s (nm)	lattice parameter(s) (Å)	D (nm)	$T\%$	$R\%$	E_g^{op} (eV)	n
Co_3O_4	17.25	$a = 8.121$	24	61.72	9.29	1.7	2.877
CuO	22.51	$a, b, c = 4.72, 3.431, 5.128$	26	62.98	23.01	1.7	2.877
IrO_2	18.55	–	–	62.21	23.01	2.2	2.654
ZnO	34.21	$a, c = 3.254, 5.21$	38	89.18	10.22	3.2	2.345
CdO	59.80	$a = 4.695$	62	78.92	6.48	2.6	2.514

3.2. Films' morphology

Fig. 3(a-c) characterizes the morphologies of Co_3O_4 , CuO , and CdO films. The 3D AFM images confirm the polycrystalline structure of these films with different grain sizes (D). It is noticeable from this figure that the surface morphology is strongly dependent upon the chemical composition of the films, where the size of individual grains and the roughness increase from Co_3O_4 , CuO , to CdO . Co_3O_4 shows a denser granular structure that offers reduced separations among the grains. 2D images indicate that all films are composed of spherical nanoparticles. The D values in nm are inserted in Table 1. D values in the range of 21–62 nm and are consistent with the calculated C_s from XRD data. Note that the small difference between C_s and D arises from the fact that AFM gives the size of the grain, measured by the distances between the visible grain boundaries, and the grain could be composed of one crystallite or more [44]. Moreover, the average root mean square roughness (R_{ms}) of the Co_3O_4 , CuO , and CdO is 14.5, 21.4, and 24.6 nm, respectively. The bright regions in 3D and 2D images show overgrown crystallites with a well-developed grain morphology.

Fig. 4 (a, b) shows the surface of ZnO and IrO_2 as seen under FE-SEM. ZnO 's surface displays a wrinkled net-work structure. At higher magnifications, the grains of this structure are round and grow preferentially along the c -axis direction, which is perpendicular to the substrates, or along the (0 0 2) direction, as noted in the XRD pattern of ZnO . The agglomerated particles are almost spherical, with an average diameter of ~ 38 nm. The surface of IrO_2 film, Fig. 4 (b), appears to have collapsed nanorods of diameters in the range of 80–120 nm and an average value of 100 nm. The height of these rods is in the range of 250–315 nm. This indicates that the average film thickness is about 284 nm.

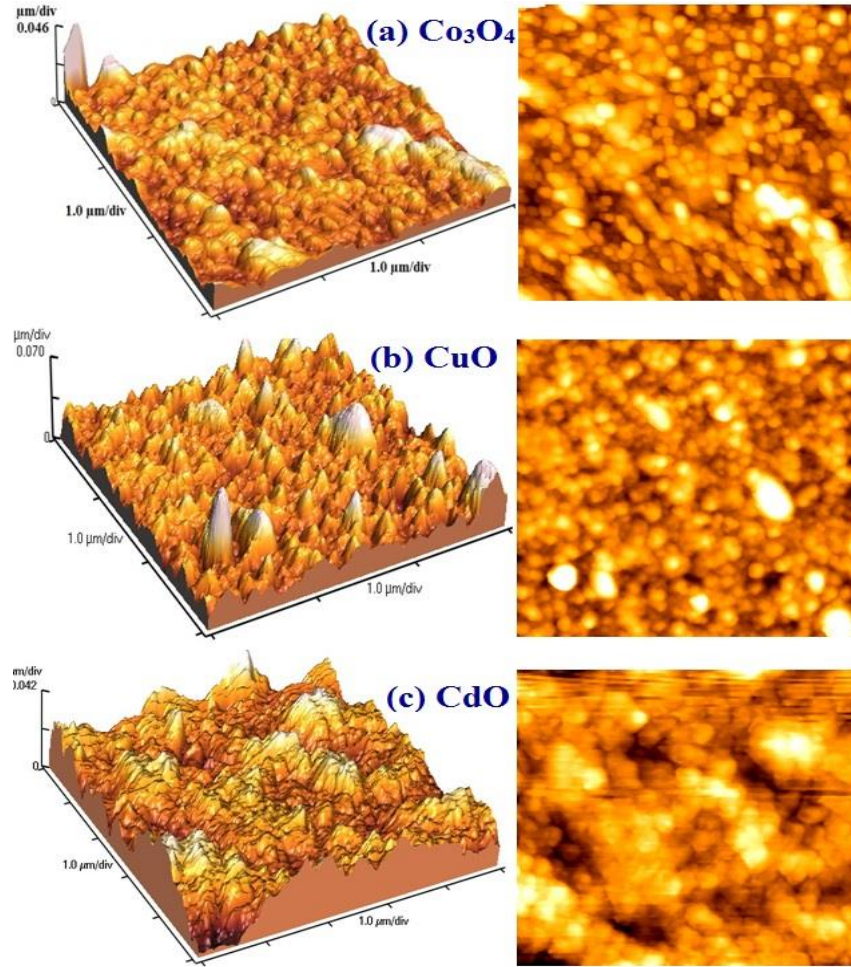


Fig.3: AFM (3D and 2D) images for the surface of Co_3O_4 , CuO , and CdO thin films.

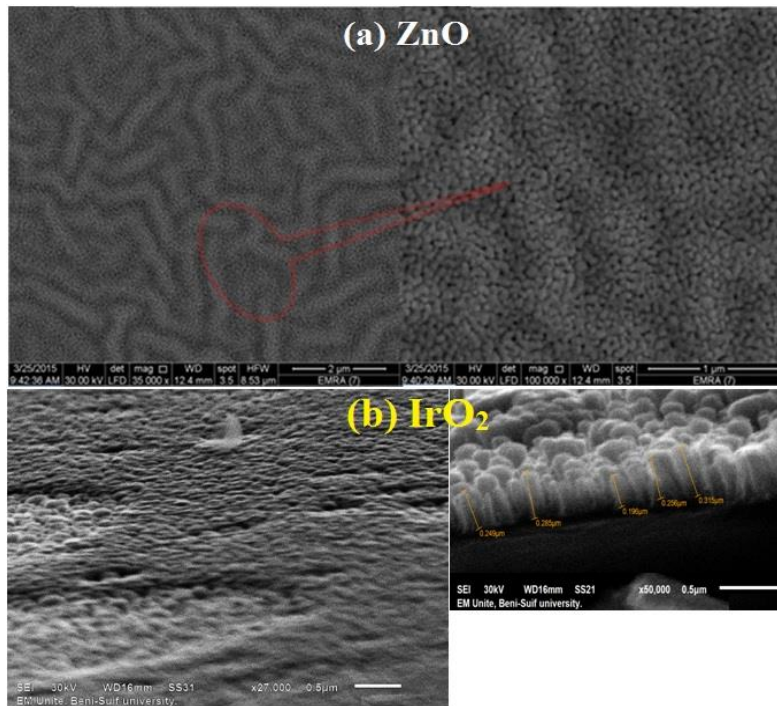


Fig. 4: FE-SEM investigation for (a) ZnO and (b) IrO_2 films.

3.3. Optical characterizations

UV-vis-NIR spectroscopy is an interesting and powerful technique for exploring the optical properties of semiconductor nanomaterials and their band structure. The transmittance (T%) and reflectance (R%) spectra of the addressed films are shown in Fig. 5(a-e). For comparison purposes, the T% and R% values at $\lambda = 700$ nm of the films are listed in Table 1. For all films, except CdO, no light is transmitted for $\lambda < 250$ nm and the films show the maximum T% in the near IR region. CdO exhibits $T > 40\%$ in the UV region. At 700 nm wavelength, Co_3O_4 , CuO, and IrO_2 thin films show T% around 62%, while the TCO (ZnO and CdO) are highly transparent (79–89%). T% spectra of Co_3O_4 and ZnO display interference fringes, indicating the layered structure of the sol-gel spin-coated films. CuO and IrO_2 films show high R% in the UV region. This indicates the possibility of using these materials to block UV rays. Moreover, CuO, IrO_2 , ZnO, and CdO exhibit high T% and very low R% in the IR region. Therefore, these materials can be tailored for sensing applications in the IR region.

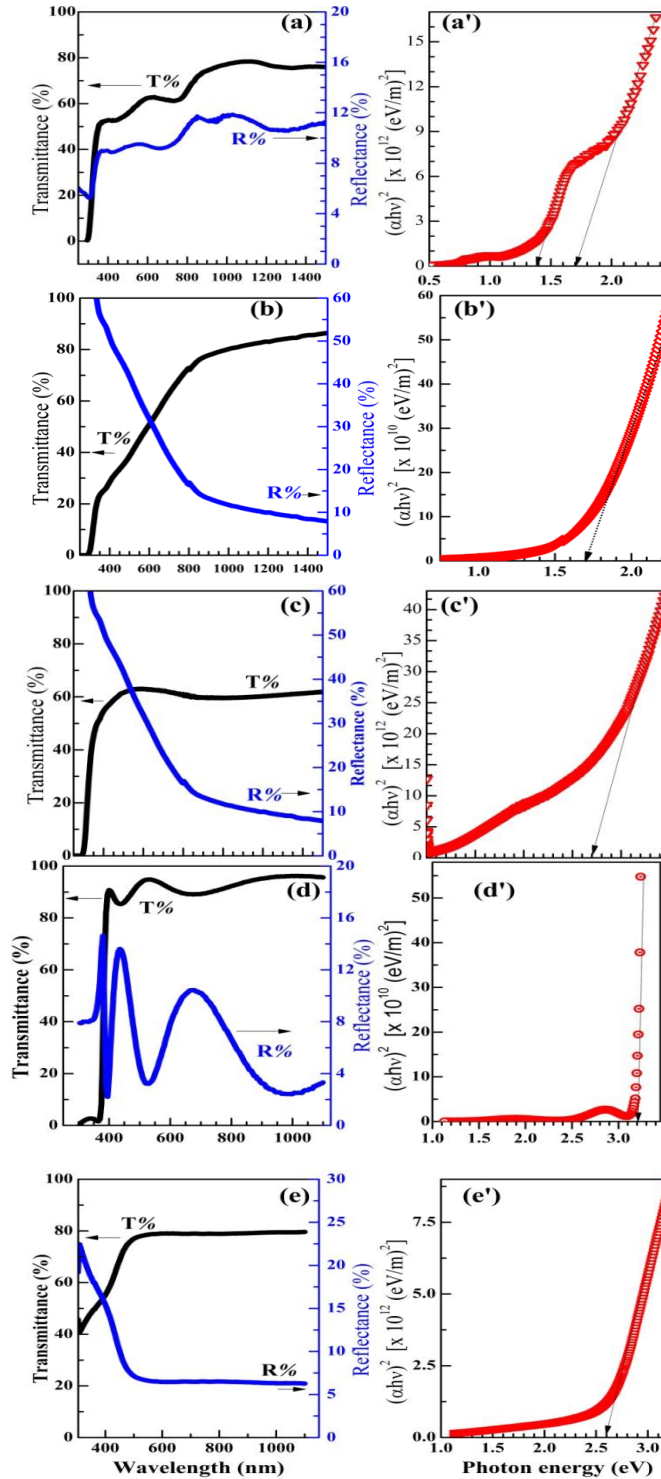


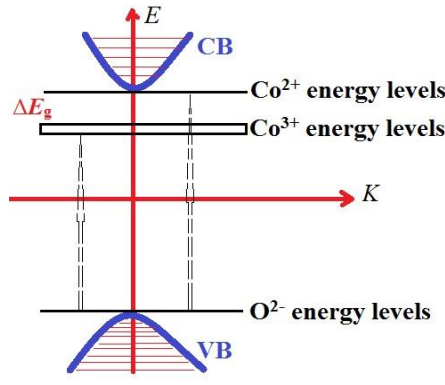
Fig.5 (a-e): Optical transmittance and reflectance spectra of the Co_3O_4 , CuO, IrO_2 , ZnO, and CdO films.

(a'-e') the E_g^{op} reflectance spectra and

The collected T and R spectra were used to calculate the absorption coefficient [45]: $\alpha = -\frac{1}{d} \ln\left(\frac{T}{1-R}\right)$, where d is the film thickness evaluated by using

AFM and FE-SEM. The E_g^{op} of the films was determined from the dependence of α on $h\nu$ (the incident photon energy) by applying the Tauc' relation for the direct and allowed transitions: $\alpha h\nu = B(h\nu - E_g)^{1/2}$, where B is the edge parameter. Fig. 5(a'-e') displays the plots of $(\alpha h\nu)^2$ vs. $h\nu$, for the synthesized nanofilms. Extrapolation of the linear regions of the curves in this figure to the $h\nu$ axis at $\alpha = 0$ gives the E_g^{op} values listed in Table 1.

The E_g^{op} of CuO, IrO₂, ZnO, and CdO are 1.7, 2.2, 3.2, and 2.6 eV, respectively. These values are consistent with those reported in the literature [13, 22, 26]. These E_g^{op} values indicate the possible use of these materials in various optoelectronic applications, including gas sensing, and water splitting for hydrogen production. In the case of Co₃O₄ film, two bandgap energies are found; $E_{gl}^{op} = 1.4$ eV and $E_{gll}^{op} = 1.7$ eV. E_{gl}^{op} is arising from to the beginning of O²⁻/Co³⁺ excitation, while the E_{gll}^{op} is owing to the interband O²⁻/Co²⁺ transition and is the true bandgap [46]. The presence of E_{gl}^{op} and E_{gll}^{op} can be interpreted as follows (see Fig. 6): a) the valence band exhibits an outstanding O 2p-character. b) The fundamental impact on the conduction band is caused by the 3d orbitals of Co²⁺. c) The presence of Co³⁺ results in an intermediate band inside the bandgap. In Co₃O₄, E_g^{op} of value ≤ 1.5 eV is associated with the charge transfer of Co³⁺ d (t_{2g}) to Co²⁺ d (t_2). E_g^{op} value ≤ 2 eV, is related to the charges transfer of O²⁻ to Co²⁺ and O²⁻ to Co³⁺ [5, 47]. These transitions again confirm the presence of the Co₃O₄ spinel phase [46, 48], which is consistent with the XRD data.



3. Fig. 6: The origin of two bandgaps (E_{gl}^{op} & E_{gll}^{op}) of Co₃O₄ films

The refractive index n , where $n = \frac{\text{speed of light in air}}{\text{speed of light in the film}}$, is an important parameter for optical communications, device fabrication, anti-reflection, and coatings applications. The value of n can be determined from the E_g^{op} of the films using the following equation [49]: $\frac{n^2-1}{n^2+2} = 1 - \sqrt{\frac{E_g^{op}}{20}}$. The determined n values are given in Table 1. All films have n in the range of 2.3–2.9, and is inversely proportional to E_g^{op} . The films with higher n values (Co₃O₄, CuO, and IrO₂) have improved reflectivity owing to the huge number of particles/unit area of the films that act as scattering centers, as seen from AFM and FE-SEM.

4. Conclusions

Co₃O₄, CuO, IrO₂, ZnO, and CdO thin films have been successfully fabricated by the sol-gel spin coating technique. XRD results indicated the formation of Co₃O₄ and CdO with cubic crystal structures and crystallite sizes of 17.25 and 59.8 nm, respectively. CuO, IrO₂, and ZnO displayed monoclinic, tetragonal, and hexagonal crystallite sizes of 22.51, 18.55, and 34.21 nm, respectively. The heat treatment at 500 °C/2h was enough to convert the acetate salt or IrCl₃, to the corresponding oxide. AFM and FE-SEM analyses indicated that the substrates were well-covered with films. All films were composed of a huge number of spherical grains except the IrO₂ film which displayed a nanorod-like morphology. The TCO films (ZnO and CdO) showed improved transmittance (79–89%) compared to the other films, which showed about 62% transmission. All films, except Co₃O₄, exhibited high reflectivity in the UV region and lower reflectivity in the IR region. In summary, five different transition metal oxides were prepared by a facile sol-gel spin coating technique. Co₃O₄ and CuO have E_g^{op} of 1.7 eV are suitable for water splitting under solar radiation for hydrogen production and also for gas sensing applications. IrO₂, ZnO and CdO films have E_g^{op} in the range of 2.2–3.2 eV are most suitable for optoelectronic applications. All of these films have a refractive index in the range of 2.3–2.9 and therefore can be exploited for coating and anti-reflection coating applications. More additional work should be performed to study the effect of deposition parameters such as solution molarity, spin speed, pre-heating, and final annealing temperatures on the morphology and optical parameters of the films. Moreover, it is expected to obtain these films with tunable properties by doping them with one or more elements during the preparation process. This will widen the film's multi-functionality and pave the way for advanced technological applications.

Acknowledgment

The authors would like to thank Fayoum University for supporting the publication of this work.

Author Contributions

All authors contributed to this work. Adel M. El Sayed prepared the thin films, completed the experimental measurements, and writing the first version. Both Mohamed Shaban and G. Said shared writing, editing the manuscript, analyzing the data, and validation. Adel M. El Sayed followed the revision and submission of the manuscript for publication.

Declaration of Competing Interest

The authors declare that they have no known competing financial interests or personal relationships that could have appeared to influence the work reported in this paper.

References

- [1] Q. Song, S. Zhou, S. Wang, S. Li, L. Xu, J. Qiu, Insights into the oxygen vacancies in transition metal oxides for aqueous Zinc-Ion batteries. *Chem. Eng. J.*, 461 (2023), 142033.
- [2] A. Krishnan, A. Swarnalal, D. Das, M. Krishnan, V.S. Saji, S.M.A. Shibli, A review on transition metal oxides based photocatalysts for degradation of synthetic organic pollutants. *J. Environm. Sci.*, In press, <https://doi.org/10.1016/j.jes.2023.02.051>
- [3] Y. Cao, Y. He, H. Gang, B. Wu, L. Yan, D. Wei, H. Wang, Stability study of transition metal oxide electrode materials. *J. Power Source* 560 (2023) 232710.
- [4] S. Jung, D.K. Nandi, S. Yeo, H. Kim, Y. Jang, J.-S. Bae, T.E. Hong, S.-H. Kim, Phase-controlled growth of cobalt oxide thin films by atomic layer deposition. *Surf. Coat. Technol.*, 337 (2018) 404–410.
- [5] H. El Aakib, J.F. Pierson, M. Chaik, C. Samba Vall, H. Ait Dads, A. Narjis, A. Outzourhit, Evolution of the structural, morphological, optical and electrical properties of reactively RF-sputtered cobalt oxide thin films with oxygen pressure. *Vacuum*, 159 (2019), 346–352.
- [6] A.M. El Sayed, M. Shaban, Morphological, surface and optical properties of spin-coated IrO_x films; the influence of spin speed, annealing, and (Cr, La) codoping. *Ceram. Int.*, 45 (2019) 8460–8470.
- [7] M. Shaban, R. Saad, A.M. El Sayed, Influence of chromium and lanthanum incorporation on the optical properties, catalytic activity, and stability of IrO_x nanostructured films for hydrogen generation. *Int. J. Hydrogen Energy* 48 (2023) 14255–14270.
- [8] M. Abdelfatah, A.M. El Sayed, W. Ismail, S. Ulrich, V. Sittinger, A. El-Shaer, SCAPS simulation of novel inorganic ZrS₂/CuO heterojunction solar cells. *Sci. Rep.*, 13 (2023) 4553.
- [9] R. Bhargav, S.P. Gairola, A. Patra, S. Naqvi, S.K. Dhawan, Improved performance of organic solar cells with solution processed hole transport layer. *Opt. Mater.*, 80 (2018) 138–142.
- [10] N. Kouidri, S. Rahmane, A. Allag, Substrate temperature-dependent properties of sprayed cobalt oxide thin films. *J. Mater. Sci.: Mater. Electron.* 30, (2019) 1153–1160.
- [11] S.G. Victoria, A.M.E. Raj, C. Ravidhas, An insight in the structural, morphological, electrical and optical properties of spray pyrolysed Co₃O₄ thin films. *Mater. Chem. Phys.*, 162, (2015) 852–859.
- [12] J. Xu, F. Huo, Y. Zhao, Y. Liu, Q. Yang, Y. Cheng, S. Min, Z. Jin, Z. Xiang, In-situ La doped Co₃O₄ as highly efficient photocatalyst for solar hydrogen generation. *Int. J. Hydrogen Energy* 43 (2018) 8674–8682.
- [13] Y. Lu, N. Zhang, Q. Zhao, J. Liang, J. Chen, Micro-nanostructured CuO/C spheres as high-performance anode material for Na-ion batteries. *Nanoscale* 7, 2770–2776 (2015).
- [14] Y. Shen, M. Guo, X. Xia, G. Shao, Role of materials chemistry on the electrical/electronic properties of CuO thin films. *Acta Mater.*, 85, 122–131 (2015).
- [15] M. Sabbaghan, A.S. Shahvelayati, K. Madankar, CuO nanostructures: Optical properties and morphology control by pyridinium-based ionic liquids. *Spectrochim. Acta A* 135, 662–668 (2015).
- [16] J.K. Rao, A. Raizada, D. Ganguly, M.M. Mankad, S.V. Satayanarayana, G.M. Madhu, Investigation of structural and electrical properties of novel CuO–PVA nanocomposite films. *J Mater. Sci.*, 50 (2015) 7064–7074.
- [17] S. Ito, Y. Abe, M. Kawamura, K.H. Kim, Electrochromic properties of iridium oxide thin films prepared by reactive sputtering in O₂ or H₂O atmosphere. *J. Vacuum Sci. Technol. B* 33, 041204 (2015).
- [18] F. Scarpelli, A. Ionescu, I. Aiello, M. La Deda, A. Crispini, M. Ghedini, E. Brunelli, S. Sesti, N. Godbert, High order in a self-assembled Iridium (III) complex gelator towards nanostructured IrO₂ thin films. *Chem. An Asian J.* 12, (20) 2703–2710 (2017).
- [19] Y.-Min Chen, T.-Wei Chung, P.-Wei Wu, P.-Chun Chen, A cost-effective fabrication of iridium oxide films as biocompatible electrostimulation electrodes for neural interface applications. *J. Alloy. Compd.*, 692 (2017) 339–345
- [20] M. Moser, C. Mondelli, A.P. Amrute, A. Tazawa, D. Teschner, M.E. Schuster, A. Klein-Hoffman, N. Lopez, T. Schmidt, J. Perez-Ramírez, HCl Oxidation on IrO₂-Based Catalysts: From Fundamentals to Scale-Up. *ACS Catal.* 3 (2013) 2813–2822.
- [21] A. Taabouche, A. Bouabellou, F. Kermiche, F. Hanini, Y. Bouachiba, A. Grid, T. Kerdjac, Properties of cobalt-doped zinc oxide thin films grown by pulsed laser deposition on glass substrates. *Mater. Sci. Semicond. Process.*, 28 (2014) 54–58
- [22] Z. Alaie, S.M. Nejad, M.H. Yousefi, Recent advances in ultraviolet photodetectors. *Mater. Sci. Semicond. Process.* 29 (2015) 16–55.
- [23] J.D. Hwang, D.H. Wu, S.B. Hwang, Inserting an i-ZnO layer to increase the performance of p-Si/n-ZnO heterojunction photodetectors. *Mater. Sci. Semicond. Process.*, 39 (2015) 132–135.
- [24] R. Vettumperumal, S. Kalyanaraman, R. Thangavel, Optical constants and near infrared emission of Er doped ZnO sol-gel thin films. *J. Lumin.*, 158, (2015) 493–500.
- [25] V. Khranovskyy, T. Ekblad, R. Yakimova, L. Hultman, Surface morphology effects on the light-controlled wettability of ZnO nanostructures. *Appl. Surf. Sci.*, 258 (2012) 8146–8152.
- [26] D. S. Raj, T. Krishnakumar, R. Jayaprakash, T. Prakash, G. Leonardi, G. Neri, CO sensing characteristics of hexagonal-shaped CdO nanostructures prepared by microwave irradiation. *Sensors Actuat. B*, 171–172 (2012) 853–859.
- [27] H. Colak, O. Turkoglu, Structural and electrical studies of Cu-doped CdO prepared by solid state reaction. *Mater. Sci. Semicond. Process.*, 16, (2013) 712–717.
- [28] B. Gokul, P. Matheswaran, R. Sathyamoorthy, Influence of Annealing on Physical Properties of CdO Thin Films Prepared by SILAR Method. *J. Mater. Sci. Technol.*, 29, (2013) 17–21.
- [29] B. Sahin, F. Bayansal, M. Yüksel, N. Biyikli, H.A. Çetinkara, Effect of coumarin concentration on the physical properties of CdO nanostructures. *Ceram. Int.*, 40, (2014) 5237–5243.
- [30] R. Balakarthikeyan, A. Santhanam, K. Vibha, M. Shkir, H. Algarni, I.M. Ashraf, M. Kumar, M.R.V. Reddy, Noticeable effect of coating temperature on Co₃O₄ thin films developed through low-cost nebulizer spray pyrolysis for photo-sensing applications. *Surf. Interfac.*, 38, (2023) 102849.

- [31] K.-C. Tso, Y.-C. Hsieh, J.-F. Lee, C.-W. Pao, P.-C. Chen, J. Ohta, P.-W. Wu, Time-resolved XAS studies reveal sequential oxidative–reductive formation of Na-doped iridium oxide films with enhanced bio-stimulating performance. *J. Mater. Chem. C*, 11(2023) 1979-1987.
- [32] G. C.-Guzmán, M. Seguel, L. Fernández, C. Caro, C. Suarez, M. Matus, C. Cifuentes, F. Bustos, K. Ariz, A photochemical approach to the synthesis of ZnO/CuO films and their application to the photocatalytic degradation of rhodamines (Rh-B and Rh-6G) under UV–Vis light irradiation. *Inorg. Chem. Communic.*, 152, (2023) 110695.
- [33] A.A. Abd El-Moula, M. Raaif, F. El-Hossary, M. Abo El-Kassem, DC pulsed plasma magnetron sputtering of CdO/Cu/CdO multilayers thin films for self-cleaning and optoelectronic applications. *J. Eur. Opt. Society-Rapid Publ.* 19, (2023) 13.
- [34] M.A. F.-Mendoza, R. C.-Perez, G. T.-Delgado, S.A. Tomas, J.G. M.-Alvarez, O. Z.-Angel, Low-temperature photoluminescence spectra of CdO–In₂O₃ thin films prepared by sol–gel. *J. Lumin.*, 130, (2010), 2500–2504.
- [35] M.A. Chougule, S.G. Pawar, P.R. Godse, R.D. Sakhare, S. Sen, V.B. Patil, Sol–gel derived Co₃O₄ thin films: effect of annealing on structural, morphological and optoelectronic properties. *J. Mater. Sci.: Mater. Electron.*, 23, (2012), 772–778.
- [36] C. Gattinoni, A. Michaelides, Atomistic details of oxide surfaces and surface oxidation: the example of copper and its oxides. *Surf. Sci. Rep.*, 70, (2015) 424–447.
- [37] J. Hu, D. Li, J.G. Lu, R. Wu, Effects on Electronic Properties of Molecule Adsorption on CuO Surfaces and Nanowires. *J. Phys. Chem. C* 114, 17120–17126 (2010).
- [38] I. Singh, R.K. Bedi, Studies and correlation among the structural, electrical and gas response properties of aerosol spray deposited self assembled nanocrystalline CuO. *Appl. Surf. Sci.*, 257, (2011), 7592–7599.
- [39] I.N. Uzgoren, B. Huner, S. Yildirim, O. Eren, E. Ozdogan, Y.O. Suzen, N. Demir, M.F. Kaya, Development of IrO₂-WO₃ composite catalysts from waste WC-Co wire drawing die for PEM water electrolyzers' oxygen evolution reactions ACS sustainable. *Chem. Eng.*, 10, 13100e11 (2022).
- [40] R. Mariappan, V. Ponnuswamy, P. Suresh, R. Suresh and M. Ragavendar, Nanostructured Gd_xZn_{1-x}O thin films by nebulizer spray pyrolysis technique: Role of doping concentration on the structural and optical properties *Superlattic. Microst.*, 59, (2013), 47–59.
- [41] M. Soylyu, O. Savas, Electrical and optical properties of ZnO/Si heterojunctions as a function of the Mg dopant content, *Mater. Sci. Semicond. Process.*, 29, (2015), 76–82.
- [42] M. Karyaooui, A. Mhamdi, H. Kaouach, A. Labidi, A. Boukhachem, K. Boubaker, M. Amlouk, R. Chtourou, Some physical investigations on silver-doped ZnO sprayed thin films, *Mater. Sci. Semicond. Process.*, 30 (2015) 255–262.
- [43] A. Tadjarodi, M. Imani, Synthesis and characterization of CdO nanocrystalline structure by mechanochemical method. *Mater. Lett.*, 65 (2011) 1025–1027.
- [44] A.M. El Sayed, S. Taha, G. Said, F. Yakuphanoglu, Controlling the structural and optical properties of nanostructured ZnO thin films by cadmium content. *Superlattices Microstruct* 65, (2014) 35–47.
- [45] J. Kneer, M. Boxberg, S. Busch, A. Eberhardt, S. Palzer, J. Wollenstein, Alterations in the complex refractive index of copper oxide thin films as sensing effect for hydrogen sulfide monitoring. *Microsyst. Technol.*, 20, (2014), 607–613.
- [46] T. Warang, N. Patel, R. Fernandes, N. Bazzanella, A. Miotello, Co₃O₄ nanoparticles assembled coatings synthesized by different techniques for photo-degradation of methylene blue dye. *Appl. Catal. B* 132–133 (2013) 204– 211.
- [47] D. Han, Y. J.-F. Gu, Z. Wang, Cobalt oxide nanorods with special pore structure for enhanced ethanol sensing performance. *J. Colloid Interf. Sci.*, 531 (2018) 320–330.
- [48] M. Shaban, A.M. El Sayed, Influence of the spin deposition parameters and La/Sn double doping on the structural, optical, and photoelectrocatalytic properties of CoCo₂O₄ photoelectrodes. *Solar Energy Mater. Sol. C.*, 217, (2020) 110705.
- [49] S. Saber, S. El-Sayed, A.M. El Sayed, Influence of Eu³⁺ on the structural, optical and electrical properties of PEO–PVA: dual bandgap materials for optoelectronic applications. *J Mater. Sci: Mater. Electron.*, 34 (2023) 406.